

Robust Self-Supervised Cross-Modal Super-Resolution against Real-World Misaligned Observations

Xiaoyu Dong¹ Jiahuan Li^{1,2} Ziteng Cui¹ Naoto Yokoya^{1,2}

¹The University of Tokyo ²RIKEN AIP

dong@ms.k.u-tokyo.ac.jp

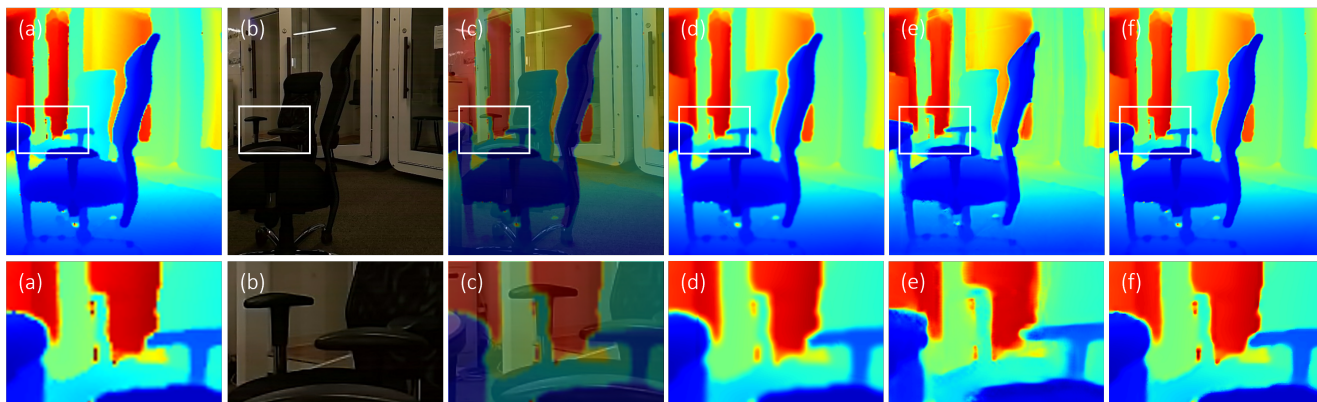


Figure 1. Real-world misaligned RGB-guided depth SR ($\times 4$). Our model achieves state-of-the-art performance *without the need for training data, ground-truth supervision, or pre-alignment*. (a) LR source; (b) HR guide; (c) pre-aligned guide by MINIMA [38]; (d) SS-GNet [45] + pre-alignment; (e) SGNNet [53] + pre-alignment; (f) RobSelf-Re (Ours).

Abstract

We study cross-modal super-resolution (SR) on real-world misaligned data, where only a limited number of low-resolution (LR) source and high-resolution (HR) guide image pairs with complex spatial misalignments are available. To address this challenge, we propose RobSelf—a fully self-supervised model that is optimized online, requiring no training data, ground-truth supervision, or pre-alignment. RobSelf features two key techniques: a misalignment-aware feature translator and a content-aware reference filter. The translator reformulates unsupervised cross-modal and cross-resolution alignment as a weakly-supervised, misalignment-aware translation subtask, producing an aligned guide feature with inherent redundancy. Guided by this feature, the filter performs reference-based discriminative self-enhancement on the source, enabling SR predictions with high resolution and high fidelity. Across a variety of tasks, we demonstrate that RobSelf achieves state-of-the-art performance and superior efficiency. Additionally, we introduce a real-world dataset, RealMisSR, to advance research on this topic. Dataset and code: [Link](#).

1. Introduction

Multi-modal images, *e.g.*, RGB, depth, and near-infrared (NIR), capture complementary properties of objects and environments [62]. However, non-visible modalities generally suffer from lower spatial resolution than RGB due to sensing and hardware limits, which hinders downstream tasks and necessitates cross-modal super-resolution (SR) [72].

Cross-modal SR enhances a low-resolution (LR) source image using structural cues from a high-resolution (HR) guide image of a different modality. Depending on data requirements, learning-based methods fall into supervised and self-supervised categories. Supervised methods [20, 53, 54, 69, 72] rely on large-scale domain-specific training data and ground truth. This reliance hinders their generalization in practice, as building such datasets is costly and labor-intensive [18]. Self-supervised methods [11, 32, 43, 45] require neither training data nor ground truth; they perform online optimization on each test source-guide pair, making them more data-efficient and generalizable.

While promising progress has been achieved, existing methods are generally developed under the assumption that the source and guide are well-aligned [11, 20, 32, 45, 53, 54, 69, 72]. In real-world scenarios, however, spa-

tial misalignment is inevitable in multi-modal images due to inherent cross-sensor discrepancies [29, 57] (e.g., differences in lens distortion, field of view, and physical position) and environmental factors, such as platform-induced viewpoint variation [22, 56] and object motion over time [28]. Although a few methods consider misalignment issues [15, 43], their alignment strategies are suboptimal, e.g., being defined solely on the guide modality overlooking cross-modal dependencies, thus limiting their performance.

We identify two major difficulties in cross-modal SR on *real-world* misaligned data: (I) The scarcity of training data and the absence of SR ground truth for the source [11, 32]; (II) Complex misalignments across modalities and resolutions, along with the lack of alignment ground truth for the guide [8, 66]. These hinder the development of reliable supervised methods. One solution is to perform pre-alignment before SR. However, such a two-stage method fails to effectively generalize real-world multi-modal images with complex misalignment and resolution gap (Fig. 1). Developing robust self-supervised cross-modal SR for real-world misaligned data is crucial yet remains an open challenge.

We address this challenge by proposing a fully self-supervised RobSelf model (Fig. 2), in which we reformulate unsupervised cross-modal and cross-resolution alignment as weakly-supervised, misalignment-aware translation. RobSelf features a misalignment-aware feature translator (Fig. 3) and a content-aware reference filter (Fig. 4). The translator aims to translate the guide to mimic the source modality while deriving an aligned guide feature with inherent redundancy. Guided by this feature, the filter performs reference-based discriminative self-enhancement on the source. Together, these techniques enable our model to achieve HR and high-fidelity predictions on real-world misaligned data, even without training data, ground-truth supervision, or pre-alignment (Fig. 1). Our model also achieves superior efficiency, up to $15.3\times$ faster than P2P [32]. In addition, we introduce the RealMisSR dataset, which provides real-world RGB-depth and RGB-NIR data featuring inherent cross-sensor misalignment, external viewpoint variation, and local object motion across diverse scenes and objects, to advance self-supervised cross-modal SR against real-world misaligned data.

The major contributions of this work include: (I) We address the open challenge of robust self-supervised cross-modal SR on real-world misaligned data by proposing the RobSelf model. (II) We collect a real-world dataset, RealMisSR, to advance research on this topic. (III) We validate RobSelf on synthesized depth SR, real-world depth SR, and real-world NIR SR, covering diverse and complex misalignments, demonstrating its robustness, generalizability, efficiency, and applicability. (IV) RobSelf achieves state-of-the-art performance, consistently outperforming previous self-supervised and supervised methods.

2. Related Work

2.1. Cross-Modal SR

Methods. Cross-modal SR has evolved from filtering [17, 31, 44], optimization [9, 13], and dictionary-based approaches [26, 49] to the learning-based paradigm. According to data requirements, learning-based methods can be categorized into supervised and self-supervised ones. Supervised methods [15, 18, 20, 34, 53, 54, 61, 69, 70, 72] rely on large-scale domain-specific training data and ground truth, whereas self-supervised methods [11, 32, 37, 43, 45, 67] are more data-efficient and generalizable, requiring no training data or ground-truth supervision. Advanced techniques such as cycle-consistent self-supervised learning [11] and self-supervised degradation learning [54] have been introduced to further enhance adaptability. However, most existing methods overlook the prevalent misalignment problem—either assuming spatially well-aligned inputs [11, 18, 20, 32, 34, 37, 45, 53, 54, 61, 67, 69, 70, 72] or adopting suboptimal alignment strategies [15, 43]. Consequently, they struggle to effectively handle real-world data that commonly exhibit complex spatial misalignments.

Datasets. Existing datasets can be grouped into purely synthetic, synthesized, and real-world ones. Purely synthetic datasets [4, 16, 36], generated by computer graphics, fail to capture real data distribution. Synthesized datasets, e.g., Middlebury [19, 39–42], NYU v2 [24], ULB17-VT [1], and EPFL RGB-NIR [3], provide HR source-guide pairs for real scenes. For this category, LR source images are synthesized by predefined degradations, which fail to reflect true LR-to-HR correspondence. Real-world datasets, e.g., ToFmark [13], FLIR One [15], RGB-D-D [18], and TOFDSR [60], contain genuine LR-HR data captured by sensors. Nevertheless, existing datasets remain limited—either unsuitable for studying the misalignment problem [1, 3, 18, 19, 24, 39–42, 48, 60] or restricted to simple cross-sensor misalignment in limited scenes [13, 15], which fail to capture the complexity and diversity of real-world misalignments.

We propose RobSelf and the RealMisSR dataset to bridge the gap in existing methods and datasets.

2.2. Multi-Modal Image Registration

Multi-modal image registration aligns images of different modalities into a common coordinate space, ensuring structure consistency for downstream tasks [27, 63]. Traditional methods [73] cast registration as heavy optimization with predefined similarity measures. Data-driven methods directly estimate transformation parameters or deformation fields in supervised [5, 7, 8, 25, 35, 38, 64, 68] and unsupervised [2, 51, 58, 59, 66] paradigms. For example, Ren *et al.* [38] proposed MINIMA, a supervised model for unified cross-modal image matching. Deng *et al.* [8] developed a

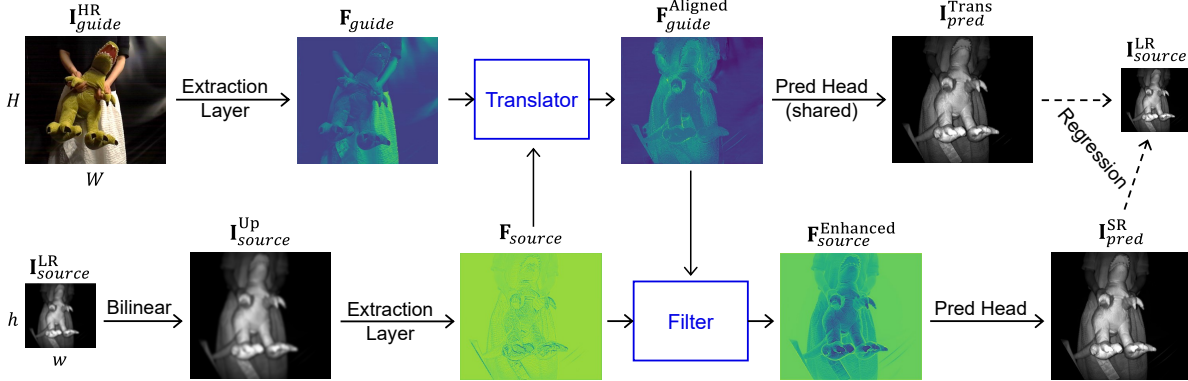


Figure 2. **RobSelf** is supervised solely by the LR source. Within this framework, the translator is weakly supervised to translate the guide feature into an HR prediction that mimics the source modality, while deriving an aligned guide feature. Guided by this feature, the filter performs reference-based discriminative self-enhancement on the source feature, from which the SR prediction is generated. Dashed flows exist only during optimization. RobSelf has **two variants depending on the alignment layer of the translator** (Sec. 3.2).

supervised model for cross-modal, cross-resolution homography estimation. Zhang *et al.* [66] performed unsupervised registration via intra-modal self-supervised learning. However, such methods rely on training domains and may fail to generalize to complex in-the-wild scenarios.

For our task, training resources are scarce and neither SR nor alignment ground truth is available. To address this, we cast unsupervised cross-modal and cross-resolution alignment as a weakly-supervised, misalignment-aware translation subtask within a self-supervised SR framework for joint online optimization. This enables strong robustness and generalizability across diverse data and misalignments.

2.3. Learnable Image Filtering

Learnable image filtering leverages data to learn filter rules or weights, enabling adaptive content modeling, suppression, and extraction [10, 55, 71]. In high-level vision, learnable filters such as tree filters [46, 47] and non-local operations [50, 52] have proven effective for modeling feature dependencies and preserving object structures. In low-level vision, non-local filters are effective in exploiting self-similarity priors to preserve structures [12], remove noise [30], and recover details [33]. In cross-modal SR, deformable filters [21], cross-domain adaptive filters [11], and degradation-aware filters [54] have been introduced to facilitate multi-modal feature fusion. However, these filters are designed for well-aligned data and may fail to transfer guidance information reliably when misalignments occur.

We observe that the guide, even after alignment (translation), contains both structures essential for enhancing the source and redundant content due to modality discrepancies. To address this, rather than filtering or fusing the guide, we design a filter that learns content-aware kernels to perform reference-based discriminative self-enhancement on the source. This enables HR and faithful SR results, free from the negative effects of redundant guide content.

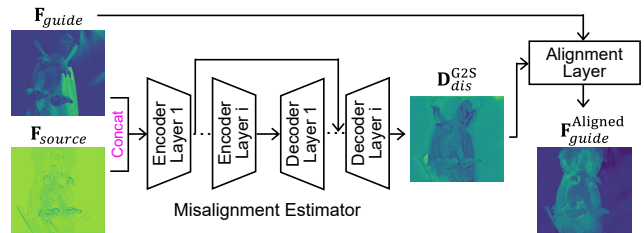


Figure 3. Misalignment-aware feature Head translator. Each encoder layer downsamples by $\times 2$; each decoder layer upsamples by $\times 2$.

3. RobSelf Model

3.1. Overview

RobSelf (Fig. 2) is fully self-supervised and features a misalignment-aware feature translator and a content-aware reference filter. Given an input image pair, the LR source $\mathbf{I}_{source}^{LR} \in \mathbb{R}^{h \times w \times \phi}$ is first bilinearly upsampled to match the spatial size of the HR guide $\mathbf{I}_{guide}^{HR} \in \mathbb{R}^{H \times W \times \psi}$. Next, two extraction layers produce the source and guide features, $\mathbf{F}_{source}, \mathbf{F}_{guide} \in \mathbb{R}^{C \times H \times W}$. ϕ, ψ , and C denote channel dimensions. The translator aligns \mathbf{F}_{guide} to \mathbf{F}_{source} , yielding the aligned guide feature, $\mathbf{F}_{guide}^{Aligned}$. Guided by $\mathbf{F}_{guide}^{Aligned}$, the filter enhances the source feature, producing $\mathbf{F}_{source}^{Enhanced}$. Based on $\mathbf{F}_{guide}^{Aligned}$ and $\mathbf{F}_{source}^{Enhanced}$, the prediction head generates $\mathbf{I}_{pred}^{Trans}$ and \mathbf{I}_{pred}^{SR} , both supervised by regression to the LR source via consistency loss [11]:

$$\mathcal{L} = \mathcal{L}_{sr} + \lambda \mathcal{L}_{trans} = \|f_{down}(\mathbf{I}_{pred}^{SR}) - \mathbf{I}_{source}^{LR}\|_1 + \lambda \|f_{down}(\mathbf{I}_{pred}^{Trans}) - \mathbf{I}_{source}^{LR}\|_1, \quad (1)$$

where f_{down} denotes average pooling. Network details are provided in the supplementary material.

3.2. Misalignment-Aware Feature Translator

To achieve translation, the translator first derives $\mathbf{F}_{guide}^{Aligned}$, which is spatially aligned to the source and contains both essential structures and redundant content.

Misalignment Estimation. The translator (Fig. 3) estimates a dense deformation field \mathbf{D}_{dis}^{G2S} that models the displacement from \mathbf{F}_{guide} to \mathbf{F}_{source} using a multi-level (i -level) estimator. With progressive downsampling and upsampling, this estimator captures misalignments across multiple spatial scales. When $i = 4$, for example, the input features are downsampled by 16 after the encoder, enabling misalignment modeling at the regional level. \mathbf{D}_{dis}^{G2S} is an $H \times W$ matrix of N -dimensional offset vectors.

Feature Alignment. The alignment layer warps \mathbf{F}_{guide} according to \mathbf{D}_{dis}^{G2S} , yielding $\mathbf{F}_{guide}^{Aligned}$. It is implemented by a deformable convolution (conv) [6] or a simple spatial resampling operation, resulting in two model variants: RobSelf-De and RobSelf-Re. At location p :

$$\mathbf{F}_{guide}^{Aligned}(p) = \begin{cases} \sum_{i=1}^{k^2} w_i \mathbf{F}_{guide}(p + p_i + \Delta p_i), & \text{if RobSelf-De,} \\ \mathbf{F}_{guide}(p + \Delta p), & \text{if RobSelf-Re,} \end{cases} \quad (2)$$

where p_i denotes the i -th relative location in the $k \times k$ conv kernel centered at p , w_i is the kernel weight, and the sampling offsets $\Delta p_i = (\Delta x_i, \Delta y_i)$ and $\Delta p = (\Delta x, \Delta y)$ are learned from \mathbf{D}_{dis}^{G2S} . Accordingly, the dimension N of \mathbf{D}_{dis}^{G2S} is $2k^2$ for RobSelf-De and 2 for RobSelf-Re.

Translation. With a prediction head (Fig. 2), the translator finally generates an HR prediction, $\mathbf{I}_{pred}^{Trans}$, weakly supervised by \mathbf{I}_{source}^{LR} to drive effective alignment and translation. Such a reformulation enables joint online optimization within a self-supervised SR framework, removing the need for costly domain-specific training as required by other registration methods, thereby achieving strong robustness and generalizability across data and misalignments.

3.3. Content-Aware Reference Filter

To better exploit essential guidance and mitigate redundancy effects, we design a filter (Fig. 4) that applies content-aware kernels to discriminatively enhance \mathbf{F}_{source} using its own pixels, with $\mathbf{F}_{guide}^{Aligned}$ only as a reference for weight determination—essentially reference-based discriminative self-enhancement.

Content-Aware Design. To achieve content discriminability, we derive an importance map $\mathbf{M}_{imp} \in \mathbb{R}^{H \times W}$:

$$\mathbf{M}_{imp} = \frac{1}{C} \sum_{c=1}^C \|\nabla(\mathbf{F}_{source}^c)\|_2, \quad (3)$$

where ∇ denotes spatial gradient operator [14], c is channel index, and C is number of channels. The motivation

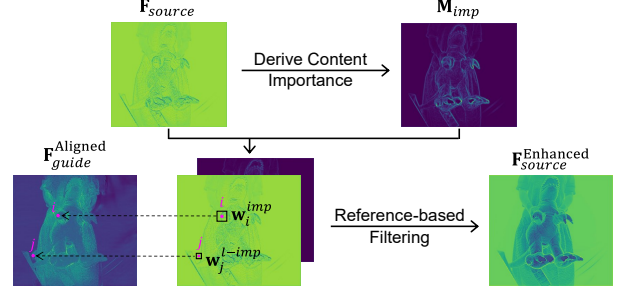


Figure 4. Content-aware reference filter.

is: high-gradient source content (e.g., edges and textures) is important, corresponding to essential guide structures; low-gradient source content (e.g., smooth regions) is less important, corresponding to redundant guide content. Depending on content importance, we adopt large and small kernels to discriminatively enhance the source pixels.

Reference-based Filtering. A threshold is computed as:

$$\tau = \eta \mathbb{E}[\mathbf{M}_{imp}], \quad (4)$$

where η is a scaling factor. For important pixels $\mathbf{F}_{source}(i)$ with $\mathbf{M}_{imp}(i) > \tau$, a *large kernel* $\mathbf{w}_i^{imp} \in \mathbb{R}^{m \times m}$ aggregates more neighbors under *stronger guidance* (essential) for effective self-enhancement; for less important pixels $\mathbf{F}_{source}(j)$ with $\mathbf{M}_{imp}(j) < \tau$, a *small kernel* $\mathbf{w}_j^{l-imp} \in \mathbb{R}^{n \times n}$ performs lightweight self-update under *weaker guidance* (redundant). We learn correlation-based kernel weights [11], proven effective in inducing pixels to emulate the properties of cross-domain references. The weights of \mathbf{w}_i^{imp} , for example, are determined by the correlation between the source pixels within an $m \times m$ neighborhood \mathcal{N}_i centered at $\mathbf{F}_{source}(i)$ and the reference pixel $\mathbf{F}_{guide}^{Aligned}(i)$ with inherent HR properties:

$$w_{i,l}^{imp} = \frac{\exp(\mathbf{F}_{source}(l)^\top \mathbf{F}_{guide}^{Aligned}(i))}{\sum_{l' \in \mathcal{N}_i} \exp(\mathbf{F}_{source}(l')^\top \mathbf{F}_{guide}^{Aligned}(i))}, \quad (5)$$

where $w_{i,l}^{imp}$ is the weight for a specific neighbor $\mathbf{F}_{source}(l)$ of $\mathbf{F}_{source}(i)$, and l' indexes all pixels within \mathcal{N}_i for normalization. The self-enhanced pixel is obtained as:

$$\mathbf{F}'_{source}(i) = \sum_{l \in \mathcal{N}_i} w_{i,l}^{imp} \mathbf{F}_{source}(l). \quad (6)$$

Such reference-based discriminative self-enhancement featuring content-aware kernels enables $\mathbf{F}_{source}^{Enhanced}$ and \mathbf{I}_{pred}^{SR} with both high resolution and high fidelity, free from the negative effects of redundant content in $\mathbf{F}_{guide}^{Aligned}$.

4. RealMisSR Dataset

We introduce RealMisSR to advance research on self-supervised cross-modal SR under misalignments. We high-

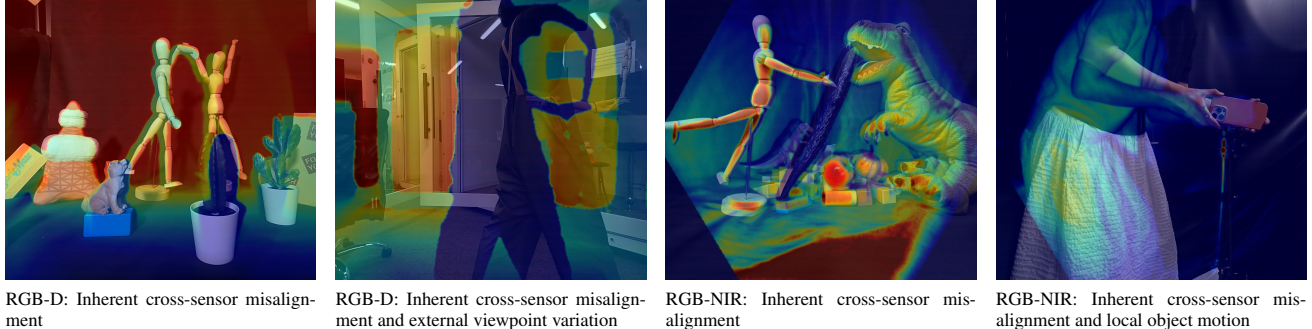


Figure 5. Example data from our RealMisSR dataset. LR sources are overlaid on HR guides for better visualization of misalignments.

Table 1. Synthesized misaligned RGB-guided depth SR. Pre-alignment is applied to methods lacking alignment strategies; results without and with this step are reported (wo/w). *Params vary with SR factors ($\times 4/\times 8$) due to level i . The **best** and **second best** are highlighted.

	P2P [32]	CMSR [43]	DCTNet [69]	MMSR [11]	SSGNet [45]	SGNet [53]	C2PD [20]	DORNet [54]	RobSelf-Re	RobSelf-De
Self-Supervised	✓	✓	✗	✓	✓	✗	✗	✗	✓	✓
Pre-Alignment	✓	✗	✓	✓	✓	✓	✓	✓	✗	✗
Params (M)	0.2	1.18	0.48	0.25	0.31	36.39	65.06	3.05	0.76/0.87*	0.81/0.92*
$\times 4$ (RMSE \downarrow)	2.81/2.33	1.91	2.19/2.16	2.22/1.88	2.20/1.92	2.44/2.33	2.12/2.06	2.57/2.46	<u>1.52</u>	1.43
$\times 8$ (RMSE \downarrow)	3.33/2.91	3.03	3.34/3.33	2.99/2.79	2.99/2.83	3.48/3.34	3.27/3.15	3.58/3.54	<u>2.57</u>	2.49

light the importance of this task in two aspects: (I) Spatial misalignment is an inherent challenge in real-world multi-modal images, in addition to resolution gaps; (II) Self-supervised models are data-efficient and exhibit strong generalizability, making them well-suited for practical scenarios where labeled training data are often unavailable.

RealMisSR (Fig. 5) features *real* LR data, two modality combinations, three types of natural misalignments, and diversity across scenes and objects. **The RGB-Depth subset** provides 52 groups of data with inherent cross-sensor misalignment (caused by factors such as sensors’ lens distortions, fields of view, and physical positions), and 60 groups of data with inherent cross-sensor misalignment and external viewpoint variation. Each group contains five images: a raw LR depth, a filled LR depth, a $\times 2$ HR depth, a $\times 2$ HR RGB, and a $\times 4$ HR RGB. The data cover small-scale toy scenes and large-scale indoor scenes, with objects such as various toys, desks, chairs, humans, and other common indoor items. **The RGB-NIR subset** provides 50 groups of data with inherent cross-sensor misalignment, and 30 groups of data with inherent cross-sensor misalignment and local object motion. Each group contains four images: an LR NIR, a $\times 2$ HR NIR, a $\times 2$ HR RGB, and a $\times 4$ HR RGB. The data span small-scale toy scenes and medium-scale human-centric scenes, with objects such as real plants, artificial plants, various toys, and humans.

For both subsets, there is no ground truth for $\times 4$ SR. The resolutions are: LR— 288×320 , $\times 2$ HR— 576×640 , and $\times 4$ HR— 1152×1280 , comparable to the RGB-D-D dataset [18], whose real-world data correspond to $\times 2.6$ SR. Further motivation statement, data collection details, and

comparisons are provided in the supplementary material.

5. Experiments

5.1. Settings

Tasks. We conduct three tasks: (I) Synthesized misaligned RGB-guided depth SR ($\times 4$, $\times 8$); (II) Real-world misaligned RGB-guided depth SR ($\times 2$, $\times 4$); (III) Real-world misaligned RGB-guided NIR SR ($\times 2$, $\times 4$). For task I, we use the Middlebury 2006 dataset [19, 39], with misalignments synthesized via random translation, rotation, and perspective shifts, and LR data generated by following [34]. For tasks II and III, we employ complex data from RealMisSR: RGB-depth with inherent cross-sensor misalignment and external viewpoint variation, and RGB-NIR with inherent cross-sensor misalignment and local object motion. Pre-alignment was performed for methods lacking alignment strategies using the official pre-trained MINIMA model [38].

Implementation. Our model is implemented in PyTorch on an NVIDIA A100 GPU. Optimization is conducted per image pair for 1000 iterations without data augmentation or translator pre-training. We adopt the Adam optimizer [23] with an initial learning rate of 0.002, decayed by 0.9998 every 5 iterations. The loss weight λ in Eq. (1) is set to 1. The misalignment estimator level i , filter threshold scaling factor η , and kernel sizes $\{m, n\}$ slightly vary with tasks to better capture the characteristics of different data. Root Mean Square Error (RMSE) or Natural Image Quality Evaluator (NIQE, no-reference) [65] is used for evaluation, depending on the availability of ground truth.

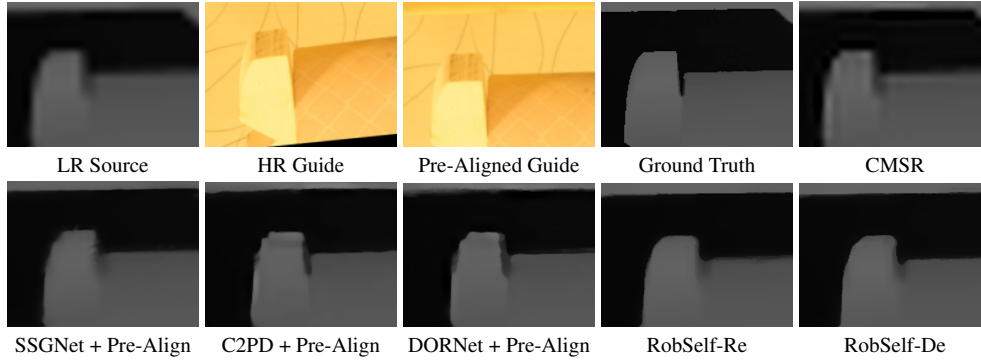


Figure 6. Synthesized misaligned RGB-guided depth SR ($\times 8$). Image patches are shown due to space limit.

Table 2. Real-World misaligned RGB-guided depth SR. Pre-alignment is applied to methods lacking alignment strategies; results without and with this step are reported (wo/w). *Params vary with SR factors ($\times 2/\times 4$) due to level i . The **best** and second best are highlighted.

	P2P [32]	CMSR [43]	DCTNet [69]	MMSR [11]	SSGNet [45]	SGNet [53]	DCNAS [72]	DORNet [54]	RobSelf-Re	RobSelf-De
Self-Supervised	✓	✓	✗	✓	✓	✗	✗	✗	✓	✓
Pre-Alignment	✓	✗	✓	✓	✓	✓	✓	✓	✗	✗
Params (M)	0.2	1.18	0.48	0.25	0.31	9.22	0.60	3.05	0.65/0.76*	0.70/0.81*
$\times 2$ (RMSE \downarrow)	3.75/3.51	2.53	3.27/3.14	2.93/2.76	2.93/2.74	3.18/2.98	3.49/3.27	3.24/3.04	<u>2.23</u>	2.18
$\times 4$ (NIQE \downarrow)	8.76/ 8.30	11.65	-/-	11.69/11.82	11.76/11.84	-/-	-/-	-/-	<u>11.24</u>	11.25

5.2. Synthesized Misaligned RGB-Guided Depth SR

The misalignment estimator level i and filter kernel sizes $\{m, n\}$ are set to 4 and $\{7, 5\}$ for $\times 4$ SR and 5 and $\{13, 7\}$ for $\times 8$ SR, with the filter threshold scaling factor $\eta = 0.7$.

Methods. We compare with four supervised methods (DORNet [54], C2PD [20], SGNet [53], DCTNet [69]) and four self-supervised methods (SSGNet [45], MMSR [11], CMSR [43], P2P [32]). The supervised methods are trained on the synthesized NYU v2 dataset [24].

Results. Table 1 reports quantitative results. On synthesized misaligned RGB-depth data, our models outperform prior methods by a large margin across SR factors, despite requiring no training data, ground-truth supervision, or pre-alignment. Figure 6 shows qualitative results. CMSR [43], limited by its suboptimal alignment strategy that overlooks cross-modal dependencies, fails to effectively enhance the source. Two-stage methods [20, 45, 54] perform better due to pre-alignment, but produce some non-faithful structures because their modules are not robust to even minor residual misalignment. In comparison, our models deliver HR and high-fidelity results, approaching the ground truth. These improvements are attributed to the joint use of our translator and filter, which effectively aligns the guide and faithfully enhances the source. The effect of our techniques is further analyzed in Sec. 5.5.

5.3. Real-World Misaligned RGB-Guided Depth SR

The misalignment estimator level i is set to 3 for $\times 2$ SR and 4 for $\times 4$ SR. The filter threshold scaling factor η and kernel

sizes $\{m, n\}$ are fixed to 0.7 and $\{7, 5\}$, respectively.

Methods. We compare with four supervised methods (DORNet [54], DCNAS [72], SGNet [53], DCTNet [69]) and four self-supervised methods (SSGNet [45], MMSR [11], CMSR [43], P2P [32]). The supervised methods are trained on the real-world RGB-D-D dataset [18].

Results. Table 2 provides quantitative results. On real-world misaligned RGB-depth data, our models achieve the best results for $\times 2$ SR. For $\times 4$ SR, RobSelf-Re ranks second in NIQE¹. It is worth noting that NIQE tends to favor results with more textures, even when such textures are spurious. This can be observed in Fig. 7, where P2P [32], despite obtaining the best NIQE score, introduces noticeable spurious textures. Other two-stage methods suffer from ghosting artifacts [53, 54] or poor boundaries [11], yielding less enhancement here than on synthesized data. This is because the pre-alignment cannot effectively generalize to these challenging real-world data, where the misalignment is more complex due to various inherent cross-sensor discrepancies and external viewpoint variation. By contrast, our models achieve strong robustness and generalizability on real-world data with complex, large misalignments, thanks to the effectiveness of our translator and the joint online optimization scheme. The effect of pre-alignment is further discussed in the supplementary material.

5.4. Real-World Misaligned RGB-Guided NIR SR

Separate prediction heads are used in this task. The misalignment estimator level i is set to 4 for $\times 2$ SR and 5 for

¹NIQE is compared only among self-supervised methods for fairness.

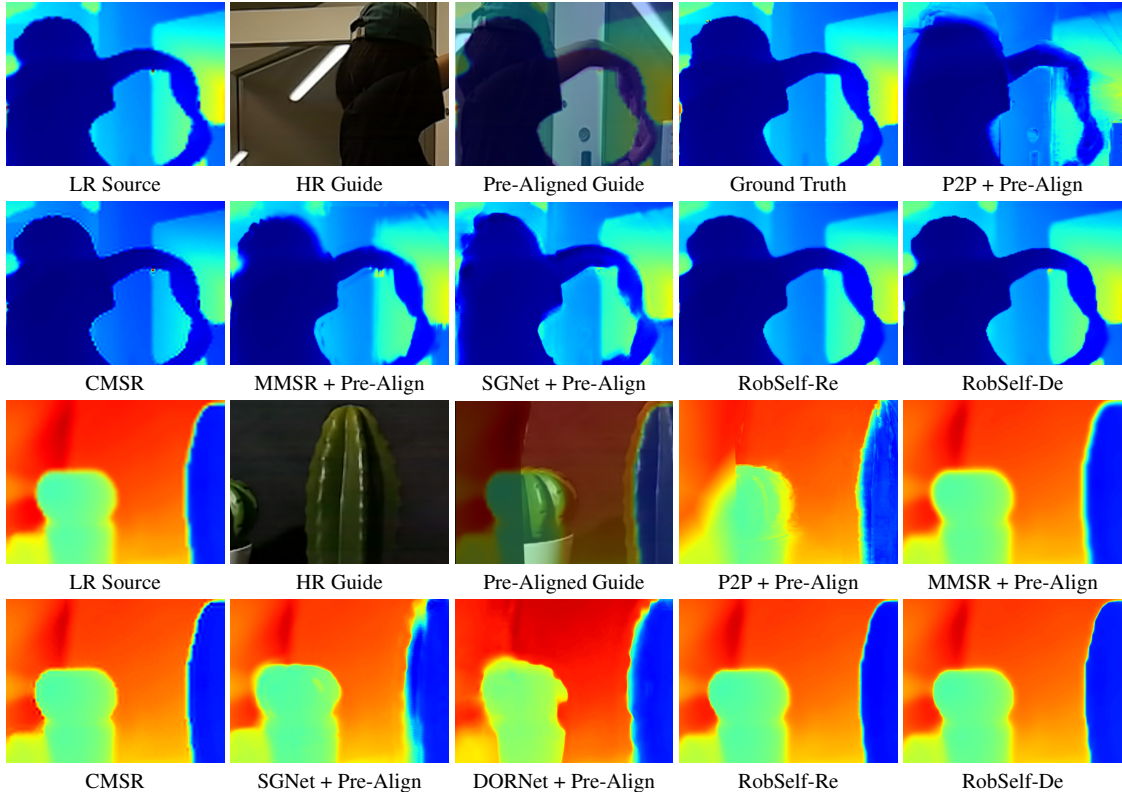


Figure 7. Real-World misaligned RGB-guided depth SR (upper: $\times 2$; lower: $\times 4$). Image patches are shown due to space limit.

Table 3. Real-World misaligned RGB-guided NIR SR. Pre-alignment is applied to methods lacking alignment strategies; results without and with this step are reported (wo/w). *Params vary with SR factors ($\times 2/\times 4$) due to level i . The **best** and second best are highlighted.

	P2P [32]	CMSR [43]	MMSR [11]	SSGNet [45]	RobSelf-Re	RobSelf-De
Self-Supervised	✓	✓	✓	✓	✓	✓
Pre-Alignment	✓	✗	✓	✓	✗	✗
Params (M)	0.2	1.18	0.25	0.31	0.91/1.02*	0.96/1.07*
$\times 2$ (RMSE \downarrow)	18.72/18.91	3.42	8.94/8.91	8.96/9.04	3.09	<u>3.12</u>
$\times 4$ (NIQE \downarrow)	6.32/ 5.32	8.05	10.95/10.50	10.30/10.23	7.63	<u>7.60</u>

$\times 4$ SR. The filter kernel sizes $\{m, n\}$ are both set to 3 to better capture the details in NIR, with no threshold applied.

Methods. We compare with prior self-supervised methods (SSGNet [45], MMSR [11], CMSR [43], P2P [32]).

Results. Table 3 and Figure 8 present quantitative and qualitative results, respectively. This task is particularly challenging due to local object motion and the rich details of NIR data. In contrast to other methods that largely degrade numerically and suffer from jagged edges (CMSR [43]), spurious textures (P2P [32]), or blur (SSGNet [45]), our models achieve more effective enhancement and recover finer spatial details. This once again demonstrates the effectiveness of our translator and filter, our models’ robustness and generalizability across data and misalignments, as well as applicability to real-world scenarios. More qualitative results are provided in the supplementary material.

5.5. Ablation Study

Here, we analyze the overall effect of our translator and filter using RobSelf-De on task II ($\times 2$ SR).

As shown in Tab. 4 and Fig. 9 (upper), when both are removed, the result remains almost unenhanced since neither the misaligned guide nor self-enhancement is effectively exploited. When only the translator is adopted, the result obtains weak enhancement due to the simple fusion of aligned guidance. When only the filter is adopted, the result obtains naive self-enhancement under misaligned guidance and introduces false structures. In contrast, when the translator is further used alongside the filter to provide aligned guidance for effective reference-based discriminative self-enhancement, the result achieves significant improvement and exhibits both high resolution and high fidelity.

Figure 9 (lower) visualizes the features from the full

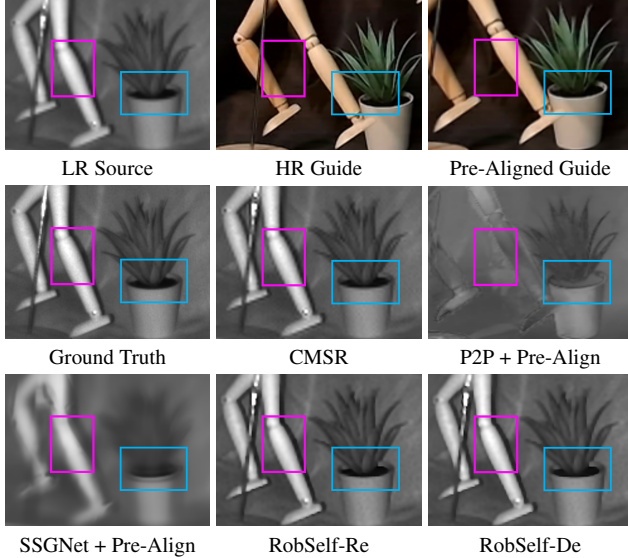


Figure 8. Real-world misaligned RGB-guided NIR SR ($\times 2$). Image patches are shown due to space limit.

Table 4. Effectiveness of our translator and filter. For the first two settings, $\{\mathbf{F}_{source}, \mathbf{F}_{guide}\}$ or $\{\mathbf{F}_{source}, \mathbf{F}_{guide}^{Aligned}\}$ are fused using a 1×1 conv. No feature fusion in the last two settings.

Translator	\times	\checkmark	\times	\checkmark
Filter	\times	\times	\checkmark	\checkmark
RMSE \downarrow	2.55	2.37	2.31	2.18

model. Our translator, by warping \mathbf{F}_{guide} and driving it to mimic the source via the weakly-supervised translation objective, effectively derives $\mathbf{F}_{guide}^{Aligned}$ that is aligned with \mathbf{F}_{source} . Since $\mathbf{F}_{guide}^{Aligned}$ and $\mathbf{I}_{pred}^{Trans}$ remain in the HR space throughout translation while supervision from LR source is applied, they preserve essential structures corresponding to the source, as well as redundant content that cannot be aligned due to modality discrepancies and is discarded in the downsampling before loss regression. To address this, our filter uses $\mathbf{F}_{guide}^{Aligned}$ as reference to determine weights for discriminative self-enhancement, which refines \mathbf{F}_{source} into $\mathbf{F}_{source}^{Enhanced}$, recovering fine details and avoiding redundancy effects. Together, our techniques provide an effective inductive bias for robust self-supervised cross-modal SR under misalignments.

See the [supplementary material](#) for more analyses, *e.g.*, alignment performance, effect of the translation objective, discriminative self-enhancement, and hyperparameters.

5.6. Runtime Efficiency

Table 5 compares the runtime (online optimization + reference) of self-supervised methods. SSGNet [45] and MMSR [11] were optimized for 1000 iterations as in our settings. P2P [32] followed its original settings to ensure

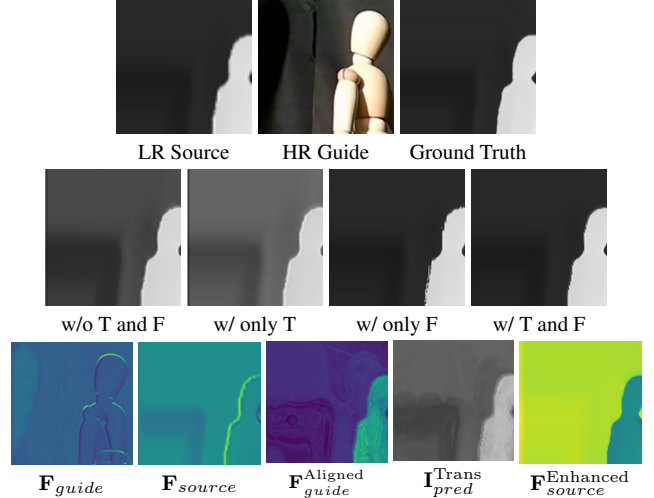


Figure 9. Effectiveness of our translator and filter.

Table 5. Average runtime on an NVIDIA A100 GPU. For SSGNet, MMSR, and P2P, RMSE with pre-alignment is reported.

	P2P [32]	MMSR [11]	SSGNet [45]	RobSelf-De	RobSelf-Re
Task I ($\times 4$). Guide: $512 \times 576 \times 3$; Upsampled source: $512 \times 576 \times 1$.					
RMSE \downarrow	2.33	1.88	1.92	1.43	<u>1.52</u>
Time	325s	137s	151s	100s	71s
Task II ($\times 2$). Guide: $576 \times 640 \times 3$; Upsampled source: $576 \times 640 \times 1$.					
RMSE \downarrow	3.51	2.76	2.74	2.18	<u>2.23</u>
Time	982s	164s	181s	122s	89s
Task III ($\times 2$). Guide: $576 \times 640 \times 3$; Upsampled source: $576 \times 640 \times 1$.					
RMSE \downarrow	18.91	8.91	9.04	<u>3.12</u>	3.09
Time	982s	164s	181s	97s	64s

performance. CMSR [43] had to be run on a different GPU due to its TensorFlow 1 code base and is therefore excluded.

Our models achieve superior efficiency. Particularly in task III, RobSelf-Re is up to $15.3\times$ faster than P2P and at least $2.56\times$ faster than MMSR and SSGNet. Such efficiency stems from our lightweight architecture and the filter, which requires no additional processing (*e.g.*, filtering and fusion) for the guide feature and employs compact kernels.

6. Conclusions

We achieve robust cross-modal SR on real-world misaligned data by proposing the fully self-supervised RobSelf model. Within RobSelf, a misalignment-aware feature translator reformulates and resolves unsupervised cross-modal and cross-resolution alignment, while a content-aware reference filter enables effective and faithful source enhancement. RobSelf demonstrates state-of-the-art performance, strong robustness and generalizability, and superior efficiency, showcasing applicability to practical scenarios where, more often than not, only limited, unlabeled misaligned data is available. We also contribute the RealMisSR dataset to facilitate further research on this topic.

References

- [1] Feras Almasri and Olivier Debeir. Multimodal sensor fusion in single thermal image super-resolution. *arXiv preprint arXiv:1812.09276*, 2018. 2
- [2] Moab Arar, Yiftach Ginger, Dov Danon, Amit H. Bermano, and Daniel Cohen-Or. Unsupervised multimodal image registration via geometry preserving image-to-image translation. In *CVPR*, 2020. 2
- [3] Matthew Brown and Sabine Süsstrunk. Multi-spectral SIFT for scene category recognition. In *CVPR*, 2011. 2
- [4] Daniel J. Butler, Jonas Wulff, Garrett B. Stanley, and Michael J. Black. A naturalistic open source movie for optical flow evaluation. In *ECCV*, 2012. 2
- [5] Si-Yuan Cao, Runmin Zhang, Lun Luo, Beinan Yu, Zehua Sheng, Junwei Li, and Hui-Liang Shen. Recurrent homography estimation using homography-guided image warping and focus transformer. In *CVPR*, 2023. 2
- [6] Jifeng Dai, Haozhi Qi, Yuwen Xiong, Yi Li, Guodong Zhang, Han Hu, and Yichen Wei. Deformable convolutional networks. In *ICCV*, 2017. 4
- [7] Xin Deng, Enpeng Liu, Shengxi Li, Yiping Duan, and Mai Xu. Interpretable multi-modal image registration network based on disentangled convolutional sparse coding. *IEEE TIP*, 2023. 2
- [8] Xin Deng, Enpeng Liu, Chao Gao, Shengxi Li, Shuhang Gu, and Mai Xu. CrossHomo: Cross-modality and cross-resolution homography estimation. *IEEE TPAMI*, 2024. 2
- [9] James Diebel and Sebastian Thrun. An application of markov random fields to range sensing. In *NeurIPS*, 2005. 2
- [10] Jiangxin Dong, Jinshan Pan, Zhongbao Yang, and Jinhui Tang. Multi-scale residual low-pass filter network for image deblurring. In *ICCV*, 2023. 3
- [11] Xiaoyu Dong, Naoto Yokoya, Longguang Wang, and Tatsumi Uezato. Learning mutual modulation for self-supervised cross-modal super-resolution. In *ECCV*, 2022. 1, 2, 3, 4, 5, 6, 7, 8
- [12] Yule Duan, Xiao Wu, Haoyu Deng, and Liang-Jian Deng. Content-adaptive non-local convolution for remote sensing pansharpening. In *CVPR*, 2024. 3
- [13] David Ferstl, Christian Reinbacher, Rene Ranftl, Matthias Ruether, and Horst Bischof. Image guided depth upsampling using anisotropic total generalized variation. In *ICCV*, 2013. 2
- [14] Rafael C. Gonzalez and Richard E. Woods. *Digital Image Processing (3rd Edition)*. Prentice-Hall, Inc., 2006. 4
- [15] Honey Gupta and Kaushik Mitra. Toward unaligned guided thermal super-resolution. *IEEE TIP*, 2021. 2
- [16] A. Handa, T. Whelan, J.B. McDonald, and A.J. Davison. A benchmark for RGB-D visual odometry, 3D reconstruction and SLAM. In *ICRA*, 2014. 2
- [17] Kaiming He, Jian Sun, and Xiaoou Tang. Guided image filtering. *IEEE TPAMI*, 2013. 2
- [18] Lingzhi He, Hongguang Zhu, Feng Li, Huihui Bai, Runmin Cong, Chunjie Zhang, Chunyu Lin, Meiqin Liu, and Yao Zhao. Towards fast and accurate real-world depth super-resolution: Benchmark dataset and baseline. In *CVPR*, 2021. 1, 2, 5, 6
- [19] Heiko Hirschmuller and Daniel Scharstein. Evaluation of cost functions for stereo matching. In *CVPR*, 2007. 2, 5
- [20] Jiahui Kang, Qing Cai, Runqing Tan, Yimei Liu, and Zhi Liu. C2PD: Continuity-constrained pixelwise deformation for guided depth super-resolution. In *AAAI*, 2025. 1, 2, 5, 6
- [21] Beomjun Kim, Jean Ponce, and Bumsub Ham. Deformable kernel networks for joint image filtering. *IJCV*, 2021. 3
- [22] Jinnyeong Kim and Seung-Hwan Baek. Pixel-aligned RGB-NIR stereo imaging and dataset for robot vision. In *CVPR*, 2025. 2
- [23] Diederik Kingma and Jimmy Ba. Adam: A method for stochastic optimization. In *ICLR*, 2015. 5
- [24] Pushmeet Kohli, Nathan Silberman, Derek Hoiem, and Rob Fergus. Indoor segmentation and support inference from RGBD images. In *ECCV*, 2012. 2, 6
- [25] Lingke Kong, X. Sharon Qi, Qijin Shen, Jiacheng Wang, Jingyi Zhang, Yanle Hu, and Qichao Zhou. Indescribable multi-modal spatial evaluator. In *CVPR*, 2023. 2
- [26] HyeokHyen Kwon, Yu-Wing Tai, and Stephen Lin. Data-driven depth map refinement via multi-scale sparse representation. In *CVPR*, 2015. 2
- [27] Huafeng Li, Zengyi Yang, Yafei Zhang, Wei Jia, Zhengtao Yu, and Yu Liu. MulFS-CAP: Multimodal fusion-supervised cross-modality alignment perception for unregistered infrared-visible image fusion. *IEEE TPAMI*, 2025. 2
- [28] Runfeng Li, Mikhail Okunev, Zixuan Guo, Anh Ha Duong, Christian Richardt, Matthew O’Toole, and James Tompkin. Time of the flight of the gaussians: Optimizing depth indirectly in dynamic radiance fields. In *CVPR*, 2025. 2
- [29] Federico Lincetto, Gianluca Agresti, Mattia Rossi, and Pietro Zanuttigh. Multimodalstudio: A heterogeneous sensor dataset and framework for neural rendering across multiple imaging modalities. In *CVPR*, 2025. 2
- [30] Ding Liu, Bihan Wen, Yuchen Fan, Chen Change Loy, and Thomas S Huang. Non-local recurrent network for image restoration. In *NeurIPS*, 2018. 3

- [31] Ming-Yu Liu, Oncel Tuzel, and Yuichi Taguchi. Joint geodesic upsampling of depth images. In *CVPR*, 2013. [2](#)
- [32] Riccardo de Lutio, Stefano D’Aronco, Jan Dirk Wegner, and Konrad Schindler. Guided super-resolution as pixel-to-pixel transformation. In *ICCV*, 2019. [1](#), [2](#), [5](#), [6](#), [7](#), [8](#)
- [33] Yiqun Mei, Yuchen Fan, and Yuqian Zhou. Image super-resolution with non-local sparse attention. In *CVPR*, 2021. [3](#)
- [34] Nando Metzger, Rodrigo Caye Daudt, and Konrad Schindler. Guided depth super-resolution by deep anisotropic diffusion. In *CVPR*, 2023. [2](#), [5](#)
- [35] Tony C. W. Mok, Zi Li, Yunhao Bai, Jianpeng Zhang, Wei Liu, Yan-Jie Zhou, Ke Yan, Dakai Jin, Yu Shi, Xiaoli Yin, Le Lu, and Ling Zhang. Modality-agnostic structural image representation learning for deformable multi-modality medical image registration. In *CVPR*, 2024. [2](#)
- [36] Martin Peris, Sara Martull, Atsuto Maki, Yasuhiro Ohkawa, and Kazuhiro Fukui. Towards a simulation driven stereo vision system. In *ICPR*, 2012. [2](#)
- [37] Xin Qiao, Chenyang Ge, Chaoqiang Zhao, Fabio Tosi, Matteo Poggi, and Stefano Mattoccia. Self-supervised depth super-resolution with contrastive multiview pre-training. *Neural Networks*, 2023. [2](#)
- [38] Jiangwei Ren, Xingyu Jiang, Zizhuo Li, Dingkan Liang, Xin Zhou, and Xiang Bai. MINIMA: Modality invariant image matching. In *CVPR*, 2025. [1](#), [2](#), [5](#)
- [39] Daniel Scharstein and Chris Pal. Learning conditional random fields for stereo. In *CVPR*, 2007. [2](#), [5](#)
- [40] Daniel Scharstein and Richard Szeliski. A taxonomy and evaluation of dense two-frame stereo correspondence algorithms. *IJCV*, 2002.
- [41] Daniel Scharstein and Richard Szeliski. High-accuracy stereo depth maps using structured light. In *CVPR*, 2003.
- [42] Daniel Scharstein, Heiko Hirschmüller, York Itajima, Greg Krathwohl, Nera Nestic, Xi Wang, and Porter Westling. High-resolution stereo datasets with subpixel-accurate ground truth. In *GCPR*, 2014. [2](#)
- [43] Guy Shacht, Dov Danon, Sharon Fogel, and Daniel Cohen-Or. Single pair cross-modality super resolution. In *CVPR*, 2021. [1](#), [2](#), [5](#), [6](#), [7](#), [8](#)
- [44] Takashi Shibata, Masayuki Tanaka, and Masatoshi Okutomi. Misalignment-robust joint filter for cross-modal image pairs. In *ICCV*, 2017. [2](#)
- [45] Jisu Shin, Seunghyun Shin, and Hae-Gon Jeon. Task-specific scene structure representations. In *AAAI*, 2023. [1](#), [2](#), [5](#), [6](#), [7](#), [8](#)
- [46] Lin Song, Yanwei Li, Zeming Li, Gang Yu, Hongbin Sun, Jian Sun, and Nanning Zheng. Learnable tree filter for structure-preserving feature transform. In *NeurIPS*, 2019. [3](#)
- [47] Lin Song, Yanwei Li, Zhengkai Jiang, Zeming Li, Xiangyu Zhang, Hongbin Sun, Jian Sun, and Nanning Zheng. Rethinking learnable tree filter for generic feature transform. In *NeurIPS*, 2020. [3](#)
- [48] Shuran Song, Samuel P. Lichtenberg, and Jianxiong Xiao. SUN RGB-D: A RGB-D scene understanding benchmark suite. In *CVPR*, 2015. [2](#)
- [49] Ivana Tosic and Sarah Drewes. Learning joint intensity-depth sparse representations. In *IEEE TIP*, 2014. [2](#)
- [50] Olga Veksler and Yuri Boykov. Sparse non-local CRF. In *CVPR*, 2022. [3](#)
- [51] Di Wang, Jinyuan Liu, Xin Fan, and Risheng Liu. Unsupervised misaligned infrared and visible image fusion via cross-modality image generation and registration. In *IJCAI*, 2022. [2](#)
- [52] Xiaolong Wang, Ross Girshick, Abhinav Gupta, and Kaiming He. Non-local neural networks. In *CVPR*, 2018. [3](#)
- [53] Zhengxue Wang, Zhiqiang Yan, and Jian Yang. SGNet: Structure guided network via gradient-frequency awareness for depth map super-resolution. In *AAAI*, 2024. [1](#), [2](#), [5](#), [6](#)
- [54] Zhengxue Wang, Zhiqiang Yan, Jinshan Pan, Guangwei Gao, Kai Zhang, and Jian Yang. DORNet: A degradation oriented and regularized network for blind depth super-resolution. In *CVPR*, 2025. [1](#), [2](#), [3](#), [5](#), [6](#)
- [55] Huikai Wu, Shuai Zheng, Junge Zhang, and Kaiqi Huang. Fast end-to-end trainable guided filter. In *CVPR*, 2018. [3](#)
- [56] Zi-Xiang Xia, Sudeep Fadadu, Yi Shi, and Louis Foucard. Robust long-range perception against sensor misalignment in autonomous vehicles. In *WACV*, 2025. [2](#)
- [57] Jijun Xiang, Xuan Zhu, Xianqi Wang, Yu Wang, Hong Zhang, Fei Guo, and Xin Yang. DEPTHOR: Depth enhancement from a practical light-weight dToF sensor and RGB image. In *ICCV*, 2025. [2](#)
- [58] Han Xu, Jiayi Ma, Jiteng Yuan, Zhuliang Le, and Wei Liu. RFNet: Unsupervised network for mutually reinforcing multi-modal image registration and fusion. In *CVPR*, 2022. [2](#)
- [59] Han Xu, Jiteng Yuan, and Jiayi Ma. MURF: Mutually reinforcing multi-modal image registration and fusion. *IEEE TPAMI*, 2023. [2](#)
- [60] Zhiqiang Yan, Yuankai Lin, Kun Wang, Yupeng Zheng, Yufei Wang, Zhenyu Zhang, Jun Li, and Jian Yang. Tri-perspective view decomposition for geometry-aware depth completion. In *CVPR*, 2024. [2](#)

- [61] Zhiqiang Yan, Zhengxue Wang, Haoye Dong, Jun Li, Jian Yang, and Gim Hee Lee. Ducos: Duality constrained depth super-resolution via foundation model. In *ICCV*, 2025. [2](#)
- [62] Bo-Wen Yin, Jiao-Long Cao, Xuying Zhang, Yuming Chen, Ming-Ming Cheng, and Qibin Hou. OmniSegmentor: A flexible multi-modal learning framework for semantic segmentation. In *NeurIPS*, 2025. [1](#)
- [63] Hao Zhang, Xuhui Zuo, Jie Jiang, Chunchao Guo, and Jiayi Ma. Mrfs: Mutually reinforcing image fusion and segmentation. In *CVPR*, 2024. [2](#)
- [64] Kaining Zhang and Jiayi Ma. Sparse-to-dense multi-modal image registration via multi-task learning. In *ICML*, 2024. [2](#)
- [65] Lin Zhang, Lei Zhang, and Alan C. Bovik. A feature-enriched completely blind image quality evaluator. *IEEE TIP*, 2015. [5](#)
- [66] Runmin Zhang, Jun Ma, Si-Yuan Cao, Lun Luo, Beinan Yu, Shu-Jie Chen, Junwei Li, and Hui-Liang Shen. SCPNet: Unsupervised cross-modal homography estimation via intra-modal self-supervised learning. In *ECCV*, 2024. [2](#), [3](#)
- [67] Siyuan Zhang, Jingxian Dong, Yan Ma, Hongsen Cai, Meijie Wang, Yan Li, Twaha B. Kabika, Xin Li, and Wenguang Hou. CDF-DSR: Learning continuous depth field for self-supervised RGB-guided depth map super resolution. *Information Fusion*, 2025. [2](#)
- [68] Yiming Zhao, Xinming Huang, and Ziming Zhang. Deep lucas-kanade homography for multimodal image alignment. In *CVPR*, 2021. [2](#)
- [69] Zixiang Zhao, Jianshe Zhang, Shuang Xu, Zudi Lin, and Hanspeter Pfister. Discrete cosine transform network for guided depth map super-resolution. In *CVPR*, 2022. [1](#), [2](#), [5](#), [6](#)
- [70] Zixiang Zhao, Jianshe Zhang, Xiang Gu, Chengli Tan, Shuang Xu, Yulun Zhang, Radu Timofte, and Luc Van Gool. Spherical space feature decomposition for guided depth map super-resolution. In *ICCV*, 2023. [2](#)
- [71] Bolun Zheng, Shanxin Yuan, Gregory Slabaugh, and Ales Leonardis. Image demoiring with learnable bandpass filters. In *CVPR*, 2020. [3](#)
- [72] Zhiwei Zhong, Xianming Liu, Junjun Jiang, Debin Zhao, and Shiqi Wang. Dual-level cross-modality neural architecture search for guided image super-resolution. *IEEE TPAMI*, 2025. [1](#), [2](#), [6](#)
- [73] Barbara Zitová and Jan Flusser. Image registration methods: a survey. *Image and Vision Computing*, 2003. [2](#)